Case Studies in Construction Materials 23 (2025) e05360

Contents lists available at ScienceDirect

Case Studies in Construction Materials

journal homepage: www.elsevier.com/locate/cscm

Development of green 3D printable cementitious composites using multi-response optimisation method

Mahfuzur Rahman [a], Dong An [a], S. Rawat [b], Richard (Chunhui) Yang [a], Y. X. Zhang [c,a,*]

[a] Centre for Advanced Manufacturing Technology, School of Engineering, Design and Built Environment, Western Sydney University, Penrith, NSW 2751, Australia
[b] School of Civil and Environmental Engineering, University of Technology Sydney (UTS), Sydney, NSW 2007, Australia
[c] School of Mechanical and Mechatronics Engineering, University of Technology Sydney, 81 Broadway, Ultimo, NSW 2007, Australia

ARTICLE INFO

Keywords:
Cementitious composites
Mix design
Multi-response material optimisation
Sustainability
3D printable cementitious composites

ABSTRACT

3D printing is a new but one of the most sustainable and revolutionary manufacturing technologies for the construction sector. The printability relies on fresh properties; hence, effective mix design requires a systematic optimisation approach. This paper, for the first time, develops a green and 3D printable cementitious composite (3DP-CC) employing the Taguchi-based TOPSIS optimisation method, and a high volume of ground granulated blast furnace slag (GGBFS) is used, in replacement of cement, which has been commonly used in 3DP-CC. The developed optimisation material design method and 3D printing materials consider nine performance criteria encompassing fresh and mechanical properties and sustainability aspects, including flowability, buildability, mini-slump, deformation, weighted mini-slump, 1-day and 28-day compressive strength, flexural strength, and CO_2 emission rate. Three factors, each with three control levels, are analysed, including GGBFS content (50 %, 60 %, 70 %), superplasticiser (SP) dosage (4, 5, 6 L/m^3 of mortar), and viscosity modifying agent (VMA) dosage (4, 8, 12 L/m^3 of mortar). The mix, with 60 % GGBFS content, SP dosage and VMA dosage of 5 L/m^3 and 8 L/m^3 is determined to be the optimal mix via using the devised optimisation method, and the optimal mix design is validated by 3D printing, demonstrating favourable printability performance.

1. Introduction

3D printing is the latest digital construction method, which has seen increasing industry adoption, revolutionising construction practices as the fundamentals of Industry 4.0 for the construction industry. This digital and automated construction method is also the most sustainable manufacturing method and it has unique advantages over traditional formwork-based construction techniques [1]. It can create complex geometrical shapes and reduce reliance on formwork, saving up to half of total construction costs [2]. Additionally, it decreases labour dependence and construction waste by optimising material usage. 3DP-CC reduces building costs by cutting construction time by 25 %, reducing manpower costs by 50–70 % and labour costs by 50–80 % [3]. It has also been reported to cut environmental impact by 50 % compared to traditional construction [4].

* Corresponding author at: School of Mechanical and Mechatronics Engineering, University of Technology Sydney, 81 Broadway, Ultimo, NSW 2007, Australia.
E-mail address: sarah.zhang@uts.edu.au (Y.X. Zhang).

https://doi.org/10.1016/j.cscm.2025.e05360
Received 26 July 2025; Received in revised form 9 September 2025; Accepted 28 September 2025
Available online 29 September 2025

For 3D printing in construction, the development and application of a 3DP-CC, which is used as ink for a 3D printing machine, is crucial and thus demands careful design. To make the mixture suitable for 3D printing, the mixture needs to meet the printability criteria and be compatible enough to have adequate buildability and extrudability, while also satisfying flowability and pumpability performance criteria. These criteria can be contradictory and need proper optimisation to create a mix, which meets all the necessary property performance criteria while exhibiting satisfactory mechanical performance to be used for real life construction works.

There is a strong need to develop mix designs for 3DP-CC that enhance sustainability by reducing the cement content, since many previous studies have relied on very high cement content (550–1000 kg/m^3) compared to 270–350 kg/m^3 in conventional concrete, which results in a significantly larger environmental footprint due to the carbon-intensive nature of cement production [5]. Fly ash (FA) has been commonly used as a replacement for OPC in 3D printing [6–8]. However this practice is expected to decrease as efforts are made to reduce coal consumption and shift towards renewable energy sources leading to reduced availability of FA [9]. There is an increasing and pressing demand of alternative supplementary cementitious materials (SCM) to be used in 3D printing mixes. Other SCMs explored as alternatives to FA include calcined clays, rice husk ash, steel slag, waste glass powder, and alum sludge from water treatment [5,10]. However, among these alternatives, GGBFS, an industrial by-product with much lower energy requirements in manufacturing and a reduced carbon footprint [11] can be an excellent solution. GGBFS enhances buildability and green strength due to its angular particle interlocking, making it highly compatible with 3D printing applications [12]. It facilitates early setting, allowing the cementitious mix to quickly attain initial strength [11]. While GGBFS improves workability, substituting OPC above 40 % reduces flowability due to increased water demand, making the paste more viscous and less pumpable [13]. Thus, use of high-volume GGBFS in 3D printing is still rare, and optimizing such a mix would be a major step toward sustainability. The proper dosages of SP and VMA are crucial in this study, as they play a key role in significantly influencing the fresh properties of the mixtures [14].

The development of 3DP-CC mix designs lacks standardised guidelines, with most research relying on trial-and-error adjustments of mix constituents (e.g., OPC, SCM, SP, water-to-binder ratio) to achieve satisfactory fresh properties [15,16]. However, these methods are unsystematic, often based on limited cases focusing primarily on a few fresh property parameters, while overlooking mechanical properties in mix design. Unlike conventional trial-and-error methods that rely on iterative adjustments and empirical observations to achieve 3D printability, this study employs a systematic and data-driven approach by integrating the Technique for Order Preference by Similarity to Ideal Solution (TOPSIS) based Taguchi optimisation for mix design. The Taguchi method is a statistical design of experiments approach that efficiently reduces the number of tests required by using orthogonal arrays, making it highly effective for screening and identifying key parameters; however, it is limited to single-objective optimisation. To overcome this, it can be integrated with multi-criteria decision-making techniques such as TOPSIS, which ranks alternatives based on their relative closeness to an ideal solution, identifying the best option as the one closest to the positive ideal and farthest from the negative ideal, while Grey Relational Analysis (GRA) converts multiple responses into a single Grey Relational Grade by evaluating how each alternative compares to the ideal response in each criterion [17]. GRA involves normalizing each response (to eliminate unit differences), calculating a Grey Relational Coefficient for each criterion (indicating the closeness of that response to the ideal), and then averaging these coefficients to obtain an overall grade [18]. VIKOR (Vlse Kriterijumska Optimizacija I Kompromisno Resenje), on the other hand, is a compromise-ranking method, which focuses on identifying a solution that is closest to the ideal while also minimizing the maximum regret among criteria. VIKOR computes a regret measure for each alternative along with an overall performance index, and ranks mixes based on an aggregated compromise solution that balances group benefit and individual regret [19].

This study represents the first-ever application of TOPSIS-based Taguchi optimisation for the development of 3D printable cementitious composites, marking a novel and significant advancement in the field. By providing a generalisable and scalable framework, this methodology enables a structured approach to mix design, making it adaptable for different material compositions and sustainability-driven modifications, ultimately surpassing the limitations of conventional heuristic-based methods. The paper is structured as follows. Section 2 provides the materials used, and Section 3 develops the TOPSIS-based Taguchi optimisation framework and outlines the performance criteria, associated factors, experimental tests conducted, and the step-by-step multi-response optimisation process. In Section 4, the optimised 3DP-CC was evaluated as per the TOPSIS-based Taguchi analysis. Finally, Section 5 validates the optimised mix design through assessments of fresh properties, mechanical properties, and direct 3D printing.

2. Materials

The 3DP-CC developed in this research includes the following ingredients – general purpose (GP) cement from Blue Circle Builders Cement, GGBFS from Builders, and silica fume (SF) from Domcrete, which were all sourced in Australia and utilised as binder materials. Locally available river sand, sieved with a 500-micron sieve, was used in a saturated surface dry (SSD) condition for the mixing process to improve printability, avoid clogging issues, and achieve better layer consistency. The SP used in this study was AVDA® 650, a high-range third generation polycarboxylic ether based high rage water reducer supplied by GCP Company. Additionally, the VMA used in this research was V-MAR® 3, produced by GCP Applied Technologies. V-MAR® 3 is a high-efficiency, ready-to-use milky white

Table 1
Chemical analysis of raw materials (wt%).

Material	SiO_2	CaO	K_2O	Al_2O_3	Na_2O	MgO	SO_3	Fe_2O_3	MnO	TiO_2
GGBFS	33.7	39.6	0.36	14.6	–	8.17	2.33	0.23	0.15	0.46
GP Cement	15.91	69.79	0.92	3.44	0.08	0.99	4.33	3.94	–	0.4
SF	96.1	0.26	0.83	0.75	0.24	0.4	0.18	0.11	–	–

liquid admixture that is used to modify the rheology of cementitious composites. V-MAR 3 complies with AS 1478 as a Type SN admixture, and it is recommended for use in conjunction with ADVA® superplasticisers used in this study. Tap water was used for preparing the mixtures. Table 1 shows the chemical composition of the GGBFS, GP cement, and SF obtained through X-ray fluorescence analysis (XRF) analysis.

Fig. 1 shows the scanning electron microscopy (SEM) images of GP cement, GGBFS and SF. The cement particles displayed irregular, rough surfaces with sharp edges, showing their crystalline nature. GGBFS particles showed a relatively smoother texture than cement particles but were more granular and angular in shape. The morphology of SF reveals predominantly spherical shapes with varying size distributions.

3. TOPSIS-based Taguchi optimisation approach

3.1. Development of the TOPSIS-based Taguchi optimisation framework

In this study, the TOPSIS-based Taguchi optimisation approach was developed as shown in Fig. 2. The primary aim of employing the TOPSIS-based Taguchi optimisation approach is to create a sustainable 3DP-CC that possesses desirable 3D printing characteristics, including flowability, buildability, and shape retention, while also delivering considerable mechanical strength, such as compressive

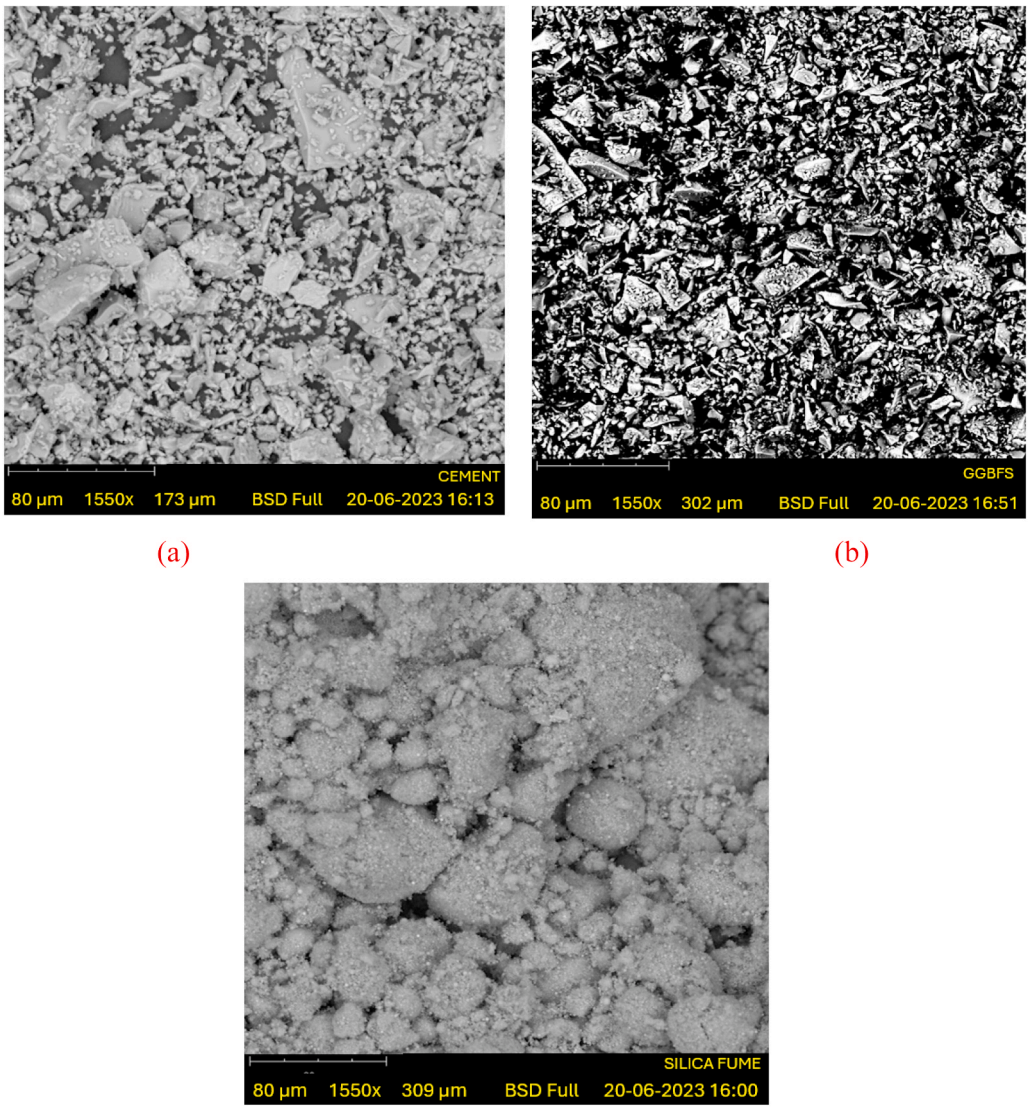

Fig. 1. SEM images of raw materials: (a) Cement, (b) GGBFS, and (c) SF.

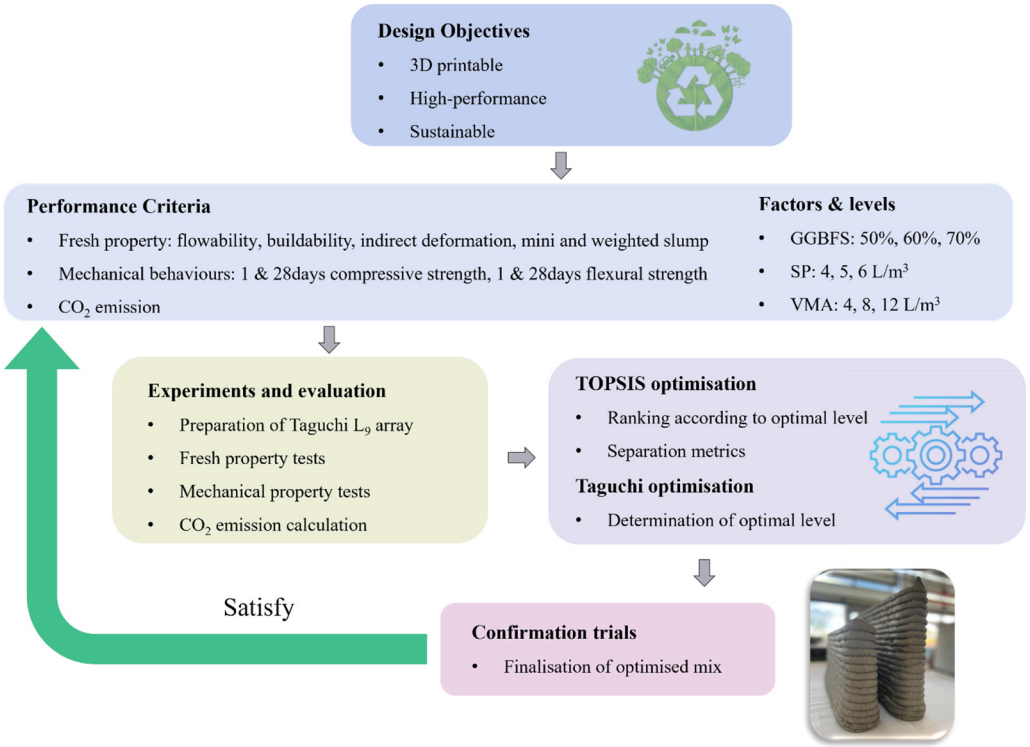

Fig. 2. TOPSIS-based Taguchi optimisation framework.

and flexural strength. In addition to optimising printability and mechanical properties, the process also prioritises sustainability by minimising CO_2 emissions. This involves calculating the CO_2 emission rate for each constituent in the mix designs under investigation, thereby promoting a reduced carbon footprint.

To analyse this process, nine performance criteria were studied, which can be categorised into fresh printability criteria, mechanical property criteria, and sustainability aspect criteria. The fresh printability criteria include flowability, buildability, mini-slump, indirect deformation, and weighted mini-slump values. The mechanical properties include 1-day and 28-day compressive strength and 28-day flexural strength results. Sustainability criteria include total CO_2 emission based per unit volume of mix constituents, which include cement usage, GGBFS usage, SF usage, and chemical admixture (SP and VMA) incorporation. Some of these criteria were aimed at maximising outcomes like mechanical strengths and flowability, while others were targeted for minimisation, such as indirect buildability spread diameter, mini-slump, deformation, weighted slump and CO_2 emission rate. Table 2 represents all 9 performance criteria, their associated symbols, and target values.

For the entire analysis, three factors were considered, with three levels for each. The factors include GGBFS content, SP, and VMA dosage. These three factors were selected because they significantly influence overall printability, sustainability, and mechanical performance. The factors and their associated levels are shown in Table 3.

The levels of SP and VMA were selected through trial tests, maintaining specified levels of GGBFS content. Reducing the SP dosage range to 4–6 L/m^3 of the mix resulted in insufficient flowability, while exceeding this range led to excessive flowability, as observed in the trials. Similarly, the VMA dosage range was analysed and set at three distinct levels. When replacing more than 70 % of cement with GGBFS, the mix became too stiff for use in a 3D printing machine. Therefore, the GGBFS content levels were limited to 50–70 % as

Table 2
Selection of performance criteria.

No	Symbol	Description	Unit	Type of Test	Target Values
1	F	Flowability	mm	Fresh printability test	Larger is better
2	MS	Mini slump	mm	Fresh printability test	Smaller is better
3	B	Buildability	mm	Fresh printability test	Smaller is better
4	ID	Indirect deformation	%	Fresh printability test	Smaller is better
5	WS	Weighted slump value	mm	Fresh printability test	Smaller is better
6	C−1	1-day compressive Strength	MPa	Mechanical test	Larger is better
7	C−28	28-day compressive strength	MPa	Mechanical test	Larger is better
8	F−28	28-day Flexural strength	MPa	Mechanical test	Larger is better
9	CE	CO_2 emission	Kg/m^3	Sustainability aspect	Smaller is better

Table 3
Selection of factors and associated levels.

Factors		**GGBFS** (% of binder) A	**SP** (L/m^3 of mix) B	**VMA** (L/m^3 of mix)C
Levels	1	50	4	4
	2	60	5	8
	3	70	6	12

a replacement for OPC.

3.2. Experimental tests

According to the mentioned-above nine performance criteria, multiple tests were conducted in this research including flowability test, mini-slump test, buildability test, indirect deformation test, compressive and flexural strength tests, etc.

3.2.1. Flowability test

The flowability test was conducted to determine the ease with which the material can be pumped through the nozzle and deposited in layers without losing its shape, which is crucial for ensuring that the mix can be efficiently printed while maintaining the desired geometrical accuracy. According to the guidelines outlined in ASTM C1437 [20] a mini-slump cone as shown in Fig. 3(a) is used for this test. All the fresh printability property tests were conducted at 30 min after the addition of water to the dry mix.

3.2.2. Mini-slump test

The mini-slump test determines whether the mix has the appropriate consistency to maintain its shape immediately after deposition. The mini-slump test was carried out following the guidelines set by ASTM C230 [21] as shown Fig. 3(b).

3.2.3. Buildability test

Measuring the spread diameter as an indirect buildability test provides valuable insights into the 3D printable mix's ability to maintain its form and support during the printing process, thereby ensuring the production of stable and high-quality printed structures. Measuring the spread diameter allows for the prediction of how well the mix will retain its shape after extrusion. A smaller spread diameter suggests higher shape stability, which is critical for the mix to support additional layers without deforming. Indirect buildability test was assessed by calculating the average spread diameter under the static load of 600 g. This method of indirect testing has also been employed in previous studies [22] and this test is referred to as an indirect buildability test as no direct 3D printing was conducted to do this test. Similar procedure to determine mini slump value was followed and finally a static load of 600 g was applied to the top surface of the cone, allowing the material to deform under this load for one minute as shown in Fig. 3(c). The spread of the material under the static load was measured in two perpendicular directions and recorded.

3.2.4. Weighted slump value and indirect deformation test

After completion of indirect buildability test the height difference of the fresh mortar from its initial height of 50 mm was measured as a weighted slump value (s') and this height is further utilised to calculate the indirect deformation of the fresh 3DP-CC. Eq. (1) is used

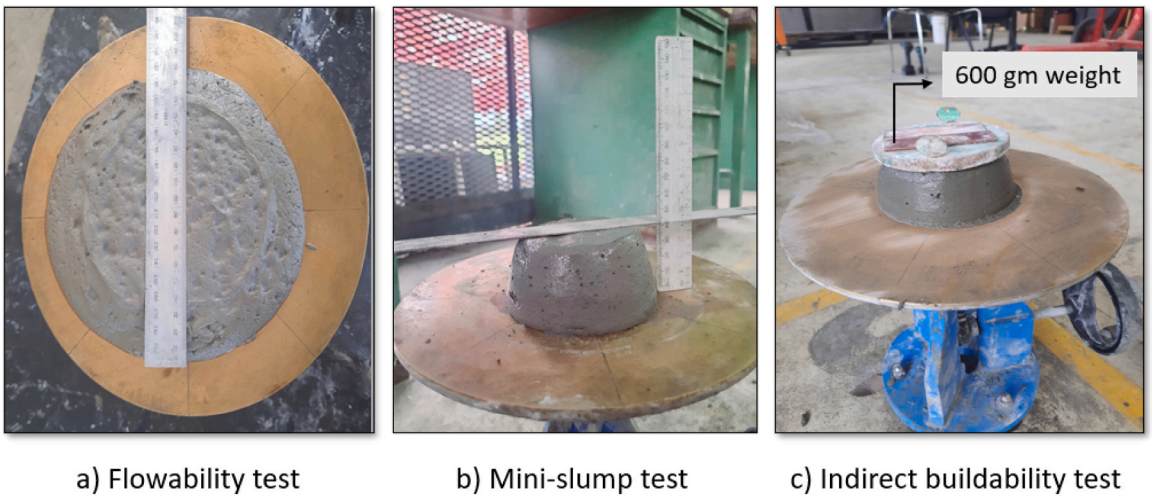

Fig. 3. Fresh property tests.

to determine the deformation percentage.

$$d = \frac{s'}{H} \times 100\% \quad (1)$$

where d indicates indirect deformation in percentages, s' represents height difference from initial height after buildability test, and H indicates the initial height of the mould, which is 50 mm.

3.2.5. Compressive and flexural strength testing

The compressive strength of mould casted specimens was tested both at 1 day and 28 days using 50 mm cubes age as per ASTM C39–21 [23] using an Instron Universal Testing Machine with a compressive capacity of 3000 kN at a loading rate of 20 MPa/min. Flexural strength test was conducted using four-point bending test, complying with ASTM C1609 with a loading rate of 0.05 mm/min [24] using the Instron 5500 R instrument incorporating 50 mm × 50 mm × 350 mm prism-sized specimens at 28 days. For both compressive strength and flexural strength tests, the average of the three specimens' test results was determined.

3.2.6. CO_2 emission analysis

The overall CO_2 emissions were calculated by considering all the mix constituents used in the study. The individual CO_2 emission rates for each mix constituent, sourced from previous studies, are presented in Table 4.

3.3. 3D printing process

3D printing was conducted using a dedicated 3D printer named 3D Potter Super 10 as shown in Fig. 4. The nozzle diameter of the printer is 25 mm. The print speed was maintained at 30 mm/min, with a nozzle stand-off distance of 12.5 mm. Beams measuring 400 mm in length and 50 mm in width were printed in 5 layers, each layer having a width of 10 mm. These printed beams were then saw-cut into the required sizes for compressive and mechanical strength testing.

A total of nine cases were investigated using the Taguchi L9 array, which is shown in Table 5.

A total of nine groups of mix designs were prepared for all the experimental investigations. The mix design for preparing 1 m^3 of the cementitious mix is shown in Table 6. In Table 6, the three factors (A: GGBFS %, B: SP dosage, and C: VMA dosage) along with their corresponding levels are denoted in the shaded portions.

3.4. Multi-response Analysis Process

3.4.1. Defining the Decision Matrix

In the TOPSIS analysis, a decision matrix is created by organising the experimental value inputs (α_{st}; s = *1, 2, 3, 4*…, representing the number of experiments *m*, *t = 1, 2, 3, 4,*…. representing the number of responses *n*). These values are arranged in a matrix form, as illustrated in Eq. (2), to serve as the decision matrix.

$$D = \begin{vmatrix} \alpha_{11} & \alpha_{12} & \dots & \alpha_{19} \\ \alpha_{21} & \alpha_{22} & \dots & \alpha_{29} \\ \dots & \dots & \dots & \dots \\ \alpha_{91} & \alpha_{92} & \dots & \alpha_{99} \end{vmatrix} \quad (2)$$

3.4.2. Normalisation Process by Linear Max-min Method

Several normalisation techniques have been documented in earlier research. For instance, Mathew et al. [29] examined the effects of six widely-used normalisation methods, such as vector, max, max-min, sum, logarithmic, and enhanced accuracy techniques, and recommended max-min as the most effective. Similarly, Sanket et al. [30] utilised the linear max-min normalisation process for multi-response optimisation of hybrid fibre-engineered cementitious composites using the grey-Taguchi method and utility concepts. This study follows a comparable strategy. For different performance criteria, if the higher values are expected in such cases it is considered as the benefit criteria, otherwise it is considered as cost criteria. Eqs. (3) and (4) provide the formulas for the selected normalisation techniques for benefit and cost criteria, respectively.

$$n^{+}{}_{i}(k) = \frac{r_i(k) - r_{i,\min}(k)}{r_{i,\max} \quad (k) - r_{i,\min}(k)} \quad (3)$$

Table 4
CO_2 emission rates for different mix constituents.

SL	Mix Constituent	CO_2 emission rate (kg CO_2/ kg of mix constituent)	Reference
1	Cement	0.90	[25]
2	GGBFS	0.143	[26]
3	SF	0.028	[27]
4	SP	2.48	[28]

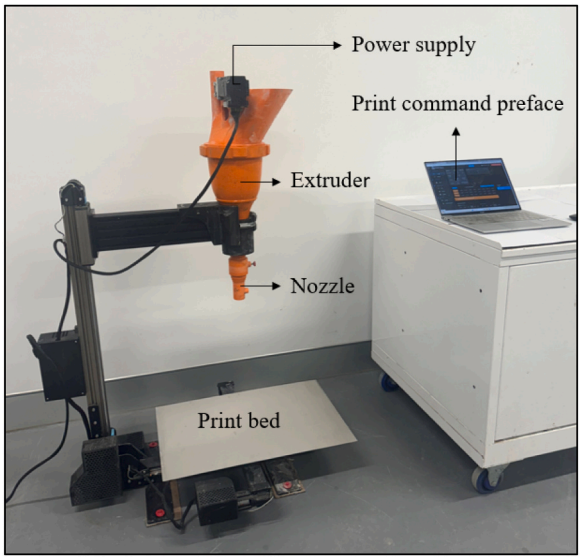

Fig. 4. 3D printing machine used in this study.

Table 5
Taguchi L9 array.

L9 Array		Process Parameter Factors	
Exp. No.	A	B	C
1	1	1	1
2	1	2	2
3	1	3	3
4	2	1	2
5	2	2	3
6	2	3	1
7	3	1	3
8	3	2	1
9	3	3	2

Table 6
Mix designs.

	Three factors			Other mix constituents						
SL	**GGBFS % (A)**	**SP (L/m^3) (B)**	**VMA (L/m^3) (C)**	**OPC %**	**SF %**	**Cement (kg/m^3)**	**GGBFS (kg/m^3)**	**SF (kg/m^3)**	**Sand (kg/m^3)**	**Water (kg/m^3)**
G1	50	4	4	40	10	508.8	636.0	127.2	462	318
G2	50	5	8	40	10	508.8	636.0	127.2	462	318
G3	50	6	12	40	10	508.8	636.0	127.2	462	318
G4	60	4	8	30	10	381.6	763.2	127.2	462	318
G5	60	5	12	30	10	381.6	763.2	127.2	462	318
G6	60	6	4	30	10	381.6	763.2	127.2	462	318
G7	70	4	12	20	10	254.4	890.4	127.2	462	318
G8	70	5	4	20	10	254.4	890.4	127.2	462	318
G9	70	6	8	20	10	254.4	890.4	127.2	462	318

$$n^{-}{}_{i}(k) = \frac{r_{i,\max}\quad(k) - r_i(k)}{r_{i,\max}\quad(k) - r_{i,\min}(k)} \tag{4}$$

In Eq. (3), $r_i(k)$ and $n_i^{+}(k)$ denote the performance value and pre-processed performance value, respectively, of the k^{th} attribute for the i^{th} alternative, considering benefit criteria. Conversely, in Eq. (4), $r_i(k)$ and $n_i^{-}(k)$ represent the performance value and pre-processed performance value for the cost criteria, respectively.

3.4.3. Determination of weighted normalised decision matrix

The weighted normalised decision matrix was determined using the equal weight method, where each performance attribute was assigned an equal weight. This analysis included a total of nine performance factors. Thus, the weighting factor $w_{(j)}$ for the j^{th} performance attribute is defined as follows:

$$w_{(j)} = [\ 0.11,\ 0.11,\ 0.11,\ 0.11,\ 0.11,\ 0.11,\ 0.11,\ 0.11,\ 0.11,\ 0.11,\ 0.11] \tag{5}$$

The weighted normalised decision matrix **U** was evaluated by Eqs. (6) and (7)

$$\mathbf{U} = [\ u_{ij}]_{m\times n} \qquad i = 1, 2, \ldots,\ m; j = 1, 2, \ldots,\ n \tag{6}$$

$$u_{ij} = \ w_j r_{ij} \quad i = 1, 2, \ldots,\ m; j = 1, 2, \ldots,\ n \tag{7}$$

3.4.4. Identification of positive ideal and negative ideal solutions

The positive ideal solution, L^+ *(L_i^+; i = 1, 2, …, k)* consists of the best values, and the negative ideal solution, L^- *(L_i^-; i = 1, 2, …, k)* consists of the worst values for the responses in the weighted normalised decision matrix. These solutions are calculated using Eqs. (8) and (9). In these equations, L^+ represents the set of cost-type criteria, while L^- represents the set of benefit-type criteria [15,21].

$$L^+ = \left\{\left(\max u_{ij} | j \in J\right),\ \left(\min u_{ij} | j \in J'\right)\right\} \tag{8}$$

$$L^- = \left\{\left(\min u_{ij} | j \in J\right),\quad \left(\max u_{ij} | j \in J'\right)\right\} \tag{9}$$

3.4.5. Calculation of the separation measures

Distance from the positive ideal solution *(D_i^+)* and from the negative ideal solution *(D_i)* are calculated by using Eqs. (10) and (11).

$$D_i^+ = \sqrt{\sum_{j=1}^{n}\left(u_{ij} - u_j^*\right)^2} \tag{10}$$

$$D_i^- = \sqrt{\sum_{j=1}^{n}\left(u_{ij} - u_j^-\right)^2} \tag{11}$$

3.4.6. Calculation of raking score

The ranking score (R_i*) is calculated using Eq. (12).

$$R_i^* = \frac{D_i^-}{D_i^- + D_i^*} \tag{12}$$

The L9 raw data matrix with all the property parameters and their results are shown in Table 7.

The normalisation matrix is derived using the max-min normalisation Eqs. (3) and (4). Subsequently, this normalised matrix is converted into the weighted normalised matrix. For this analysis, the equal weight method was employed, assigning a weight factor of 0.11 (Eq. 5) to each performance criterion. The weighted normalised matrix is then obtained using Eqs. (6) and (7), as presented in Table 8.

From the weighted normalised matrix, the positive and negative ideal solutions are calculated using Eqs. (8) and (9). Using the positive and negative ideal solutions, the corresponding separation measures – the distance from positive and negative ideal solutions were determined using Eqs. (10) and (11). Using both positive and negative values for each group of this analysis, the ranking score, which is also termed relative closeness, is determined using Eq. (12). The separation measures reflect how close each mix group is to both the best and worst possible outcomes. In this case, all groups have the same distance from the positive ideal (0.33), but their distances from the negative ideal vary slightly. This variation affects the relative closeness (Ri*), which shows how well each group performs overall. A higher Ri* means the group is closer to the optimal mix. Based on the results in Table 9, Group G9 stands out with the highest closeness score of 0.57, indicating the most favourable combination, followed by Groups G8 and G7. Table 9 exhibits the

Table 7
Raw data matrix.

Group	F	MS	B	ID	WS	C-1	C-28	F-28	CE
G1	162.5	3	100	8	4	8.6	56.7	4.9	576.2
G2	185	5	101	12	6	9.0	59.3	5.4	591.1
G3	235	13	118	38	19	7.5	54.4	4.5	606.0
G4	155	3	100	10	5	7.8	50.3	3.5	455.5
G5	178	4	100	10	5	8.8	56.1	5.1	470.4
G6	190	7	112	26	13	7.3	52.1	2.4	449.5
G7	140	1	100	6	3	6.9	41.5	2.5	334.7
G8	157.5	2	100	12	6	5.7	44.5	2.9	313.9
G9	175	5	105	14	7	7.0	47.6	4.0	328.8

Table 8
Weighted normalised matrix.

Group	F	MS	B	ID	WS	C-1	C-28	F-28	CE
G1	0.03	0.02	0.00	0.10	0.10	0.02	0.02	0.09	0.01
G2	0.05	0.04	0.01	0.09	0.09	0.00	0.00	0.11	0.01
G3	0.11	0.11	0.11	0.00	0.00	0.05	0.03	0.08	0.00
G4	0.02	0.02	0.00	0.10	0.10	0.04	0.06	0.04	0.06
G5	0.04	0.03	0.00	0.10	0.10	0.01	0.02	0.10	0.05
G6	0.06	0.06	0.07	0.04	0.04	0.06	0.04	0.00	0.06
G7	0.00	0.00	0.00	0.11	0.11	0.07	0.11	0.00	0.10
G8	0.02	0.01	0.00	0.09	0.09	0.11	0.09	0.02	0.11
G9	0.04	0.04	0.03	0.08	0.08	0.07	0.07	0.06	0.11

separation measures, relative closeness, and raking scores of all the groups.

4. Optimal mix design

The average numerical values of all the fresh and mechanical property performance parameters are displayed in Figs. 5 and 6, respectively. These values illustrate the variation pattern of the chosen factors at different levels and their individual best settings. For certain fresh property parameters such as indirect buildability, deformation percentage, and mini-slump, lower values are desirable for better printability, whereas higher values are preferred for all mechanical performance parameters. When a specific factor contributes to an individual performance parameter positively, it may, at the same time, negatively impact other performance parameters. Therefore, determining the optimal level of any particular factors depends on the average of all performance parameters rather than considering only any specific one.

It is clear from Fig. 5 that as the GGBFS content increases, the average flowability values decrease respectively. The decrease in flowability is attributed to the angular particles of GGBFS [31]. These particles have lower sphericity, which leads to increased inter-particle friction and a larger specific surface area compared to cement particles. This results in greater adsorption of water molecules on their surface, reducing the amount of free water in the fresh paste and contributing to the decrease in flowability [31]. The impact of SP dosage on flowability is highly prominent. As SP dosage increases, flowability rapidly improves due to the reduction in attractive forces between cement particles [14]. However, the effect of VMA dosage on flowability was not as significant as SP. For instance, while increasing the VMA dosage from 4 L/m^3 to 8 L/m^3, there was no significant effect on flowability, which remained around 170 mm for both dosages as shown in Fig. 5.

Increasing the GGBFS content led to a decrease in buildability spread diameter, mini-slump, indirect deformation, and weighted mini-slump values. Conversely, an increase in SP dosage resulted in higher buildability spread diameter, mini-slump, and deformation values, signifying a deterioration in overall printability. Specifically, raising the SP dosage from 5 L/m^3 to 6 L/m^3 resulted in increases of 0.3 %, 57.5 %, 41.2 %, and 41.75 % in buildability spread diameter, mini-slump, indirect deformation, and weighted slump values respectively. A more pronounced increase was observed when the SP dosage was raised from 5 L/m^3 to 6 L/m^3 , with increments of 11.26 %, 127.5 %, 130 %, and 41 % in the respective performance parameters, ultimately leading to deterioration in printability aspects. However, for flowability, the increment of SP dosage produced desirable outcomes by making the raw cementitious mix more flowable as well as pumpable. Interestingly, VMA demonstrated a dual effect on these fresh performance parameters. Initially, increasing the VMA dosage from 4 L/m^3 to 8 L/m^3 led to slight reductions of 1.92 % in buildability, 21.7 % in indirect deformation, and 21.7 % in weighted slump value. Further increases in VMA dosage resulted in 3.92 % higher buildability, 33.3 % greater deformation, and a 50 % increase in weighted slump value. Thus, from the perspective of fresh property performance, a VMA dosage of 8 L/m^3 appears to be optimal.

Fig. 6 illustrates the effects of various factors on three mechanical performance criteria: 24-hour compressive strength, 28-day compressive strength, and 28-day flexural strength. Increasing the GGBFS content in replacement of cement resulted in a reduction in both compressive and flexural strength, consistent with previous studies [32]. Higher GGBFS content leads to more partially hydrated grains, increased voids, and reduced CaO, which negatively impacts the overall hydration process and consequently reduces

Table 9
Separation measures, relative closeness, and ranking scores.

Group	Distance to positive ideal solution S+	Distance to negative ideal solution S-	Relative closeness R_i^*
G1	0.33	0.18	0.43
G2	0.33	0.18	0.43
G3	0.33	0.22	0.50
G4	0.33	0.17	0.45
G5	0.33	0.19	0.46
G6	0.33	0.16	0.44
G7	0.33	0.23	0.51
G8	0.33	0.22	0.53
G9	0.33	0.21	0.57

Table 10
Optimised mix design.

GGBFS % (A)	SP (L/m3) (B)	VMA (L/m3) (C)	Cement %	SF %	Cement (kg/m^3)	GGBFS (kg/m^3)	SF (kg/m^3)	Sand (kg/m^3)	Water (kg/m^3)
60	5	8	30	10	381.6	763.2	127.2	462	318

mechanical strength [30]. Similar trends were observed for 24-hour compressive strength and 28-day flexural strength. Regarding SP dosage, a dosage of 5 L/m^3 achieved higher mechanical strengths compared to lower (4 L/m^3) and higher (6 L/m^3) dosages. A similar pattern was observed with a VMA dosage of 8 L/m^3 , which consistently exhibited higher mechanical strength across all performance criteria. From a mechanical perspective, SP dosage of 5 L/m^3 and VMA dosage of 8 L/m^3 appear to be optimal levels.

Utilising the TOPSIS technique, all identified performance metrics were amalgamated into a unified matrix, serving as a comprehensive performance indicator in multi-variable optimisation endeavours. Additionally, the average responses across different factor levels were determined using Taguchi method. Considering the "larger the better" effects, the optimal parameter design was identified as A2 B2 C2, as illustrated in Fig. 7. All three factors, A2, B2, and C2, align at the second level, establishing the finalized Optimised design factors of GGBFS of 60 %, SP dosage of 5 L/m^3 and VMA dosage of 8 L/m^3 of cementitious mortar mix as outlined in Table 4. The Optimised mix design was finalized as shown in Table 9.

5. Experiment validation

To validate the optimal design method, the developed optimised (OPT) mix was further tested for all fresh and mechanical properties, and the results were compared with the nine initial mix designs used in the TOPSIS-based Taguchi optimisation. Since the OPT mix was developed based on the initial nine mixes, its behaviour can be more accurately assessed through comparison with these mixes. It is important to note that the optimised mix may not necessarily outperform all other mixes in every performance aspect. Instead, it exhibits a balanced performance across all parameters, making it the most suitable choice, as demonstrated by comparison with the nine mixes by dint of fresh property, mechanical property specifically through direct 3D printing.

5.1. Fresh properties of the optimal mix comparing with other mixes

The results of the fresh property test are shown in Fig. 8. In respect of flowability aspect, the OPT mix successfully achieved flowability of 180 mm at 30 min after adding water to the dry mix. Rahman et al. [14] recommended a flowability range of 160–200 mm for optimal printing performance, which was the target range for the investigated mixes in this study, and the OPT mix successfully falls in the recommended range. However, some mixes, such as G3, exceeded the optimum flowability range with a value of 235 mm, while others, such as G4, G7, and G8, showed flowability values of 155 mm, 140 mm, and 157.5 mm, respectively, which are below the targeted values and not acceptable. So, optimisation has been effective, regarding flowability performance. Through the indirect buildability test, the spread diameter served as an indirect indicator of buildability performance. A spread diameter of 100 mm represented good buildability, whereas an increase in spread diameter values indicated deteriorating buildability performance. The indirect buildability test results are shown in Fig. 8(b). Among all the investigated mixes, G3 and G6 exhibited excessive spread diameter values of 118 mm and 112 mm, respectively, 30 min after mixing, signifying unsatisfactory buildability performance. In contrast, the optimised mix demonstrated satisfactory buildability performance with a spread diameter value of 100 mm.

Regarding the mini-slump test, the optimal slump value range for 3D printability should fall within 2 mm to 12 mm for any cementitious mixture at the specified time for 3D printing, as recommended by Tay et al. [24]. Among all the mixes, G3 (13 mm) and G7 (1 mm) fall outside this recommended range as illustrated in Fig. 7(c). The OPT mix, however, demonstrated a slump value of 3 mm, indicating a satisfactory shape retention capacity, higher than most other mixtures. Additionally, Fig. 8(d) shows that the OPT mix exhibits only 8 % deformation, outperforming almost all other mixes.

Therefore, based on various fresh property tests, the optimisation process for developing a 3D printable mix has been successful.

5.2. Mechanical properties of the optimal mix compared with other mixes

The results of the mechanical property test are shown in Fig. 9. From Fig. 9(a), it is evident that the optimised mix provides a 1-day compressive strength of 8.8 MPa and a 28-day compressive strength of 56.2 MPa. Although the G2 and G1 mixes exhibit slightly higher 28-day compressive strengths (59.3 MPa and 56.73 MPa, respectively) compared to the OPT mix, both contain a lower GGBFS content of 50 %. In contrast, the OPT mix features a lower OPC content of 40 % and a higher GGBFS content of 60 %, contributing to a more sustainable mix design while maintaining a comparable 28-day compressive strength. In comparison, other mixes with a similar GGBFS content of 60 %, such as G4, G5, and G6, exhibited 28-day compressive strengths of 50.33 MPa, 53.59 MPa, and 52.08 MPa, respectively, all of which are lower than the strength achieved by the OPT mix. This underscores the success of the proposed optimisation process in significantly enhancing mechanical performance. The satisfactory improved results from both the compressive and flexural strength tests validate the success of the TOPSIS-based Taguchi optimisation method.

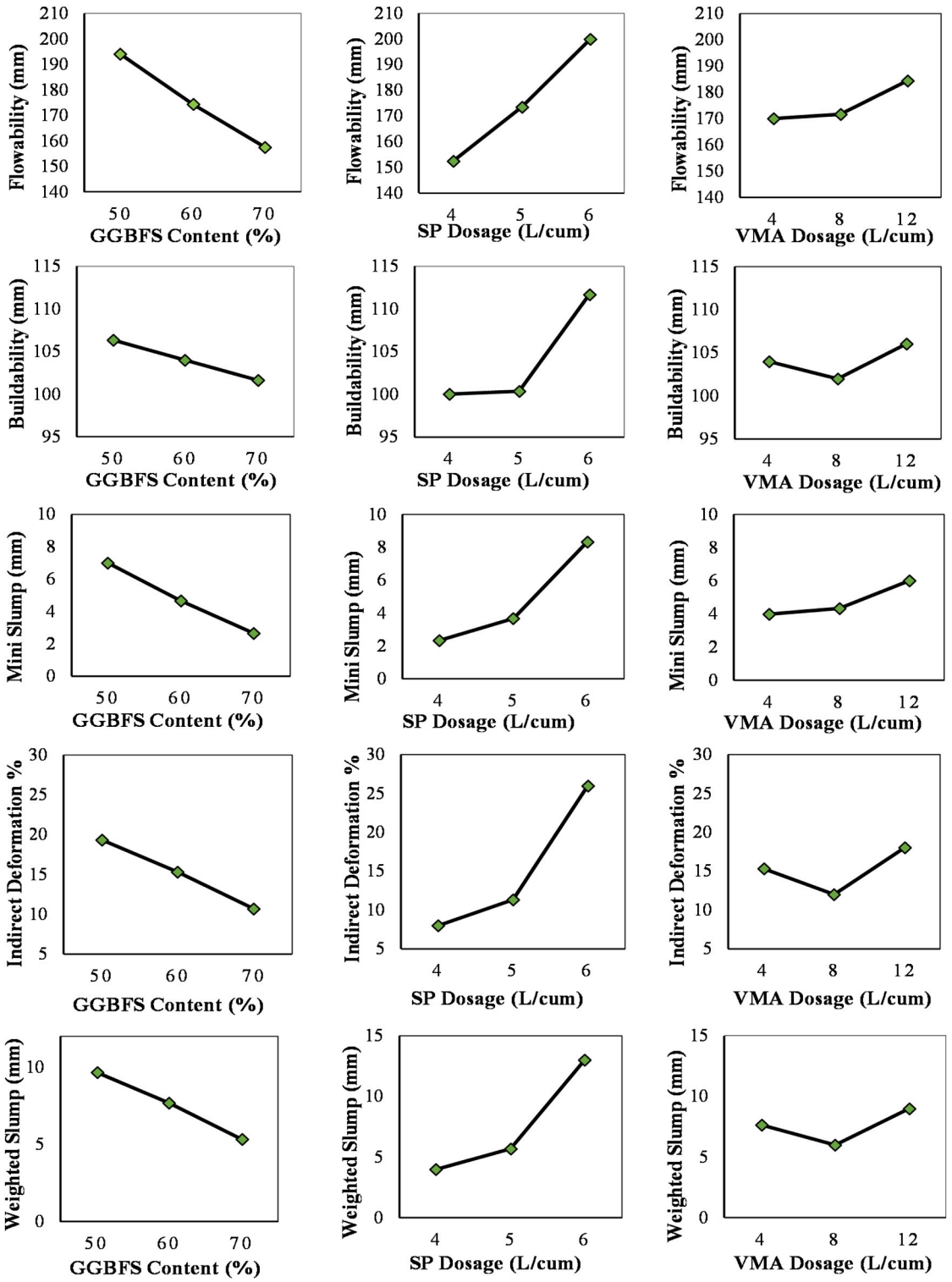

Fig. 5. Mean response of the main effect of different factors on the fresh properties.

5.3. 3D printing of the optimal mix

Direct 3D printing was performed to validate the Optimised 3D printable mix design. In addition to the Optimised mix, a reference mix consisting of 90 % OPC and 10 % SF was also printed to assess the effectiveness of the Optimised mix developed in this study.

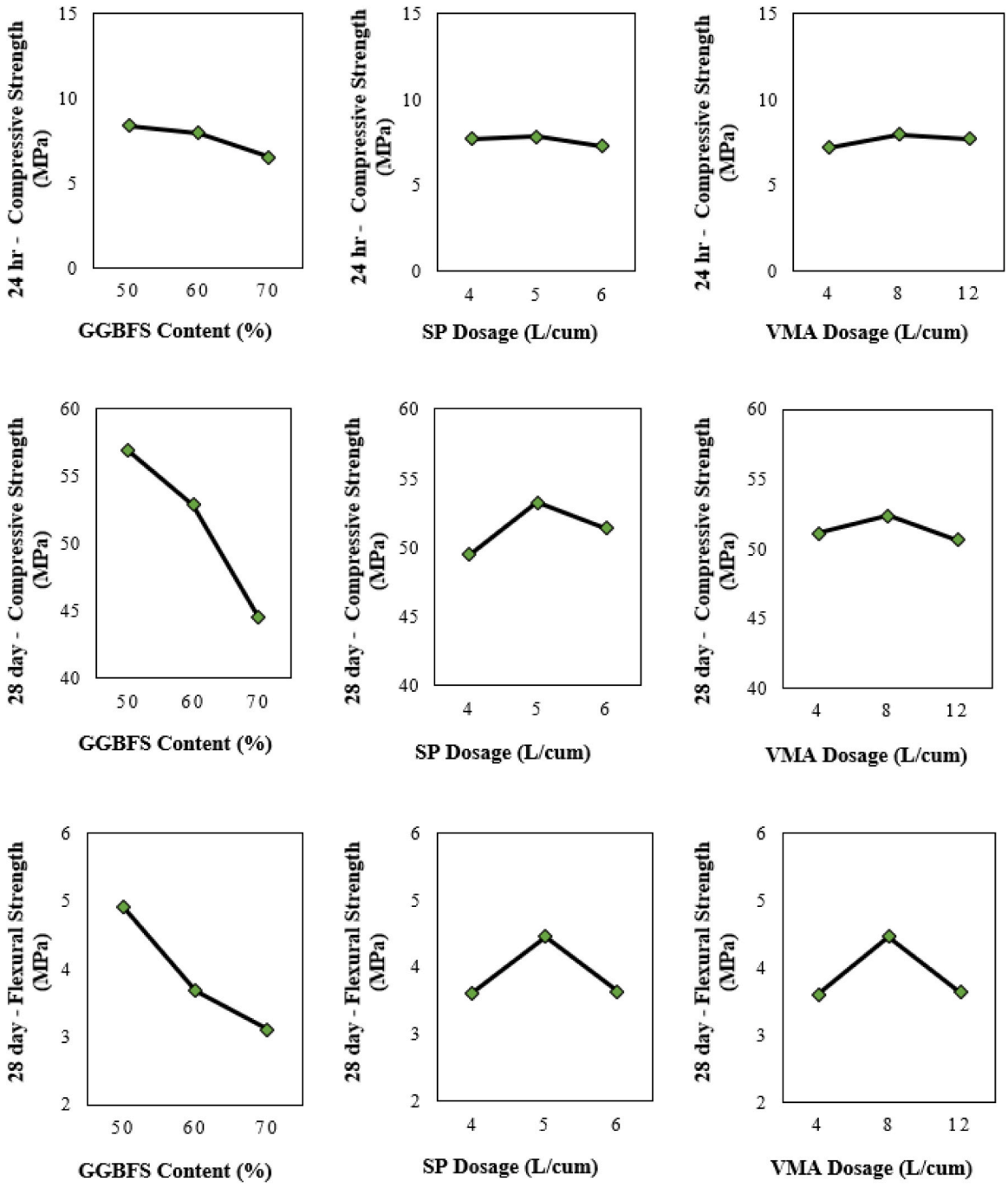

Fig. 6. Mean responses of the main effects of different factors on the mechanical properties.

Previous studies have used similar binder contents [33,34]. For a proper comparison, all printing parameters were kept constant in both cases, with the only variable being the binder composition. This approach allowed for an effective evaluation of the printability performance of the high-volume GGBFS-based sustainable 3D printable mix compared to the commonly used mix with a high cement content (90 %). The printability results of both two mixes are shown in Fig. 10.

For the OPT mix design, 20 layers were successfully printed without any buckling or collapse, achieving a total print height of 245 mm as shown in Fig. 10(a). No overlapping, cracks, or discontinuities were observed in any of the layers up to the 20th layer. Overall, these characteristics clearly demonstrate the satisfactory printability performance of the OPT mix. In contrast, the reference mix containing 90 % OPC and 10 % SF exhibited poor buildability and shape retention from the beginning, especially when compared to the OPT mix. After printing 13 layers, the reference mix became completely unstable, losing its shape retention and collapsing onto

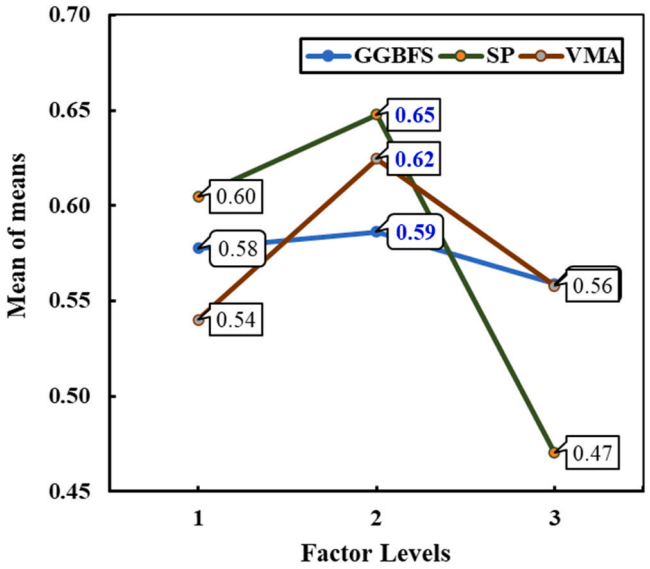

Fig. 7. Optimum factor's levels and mean plots for factor effects.

the print bed, as shown in Fig. 10 (c) and (d). Therefore, in terms of the total number of printed layers, the OPT mix significantly outperformed the reference mix. The superior printability performance of the OPT mix can be attributed to the high volume of GGBFS (60 %). The angular particles of GGBFS enhance buildability and contribute to early strength gain, both of which are advantageous for 3D printing applications [11,12,35]. The comparative printability performance validates the effectiveness of the TOPSIS-based Taguchi analysis used in the optimisation process.

6. Conclusion and Future Research

Given the numerous factors in developing 3DP-CC, it is crucial to employ a systematic approach to identify optimal mix design and evaluate the most significant factors within specific constraints. This study successfully applied a multi-response TOPSIS-based Taguchi optimisation method to investigate these factors and determine the best mix for a sustainable 3DP-CC, considering both fresh and mechanical property aspects. The following conclusions are drawn from the investigation:

- The proposed TOPSIS-based Taguchi optimisation process has proven to be effective and successful in designing a 3DP-CC mix. The results indicate that this methodology effectively determines the mixture proportions for creating a 3D printable mix with satisfactory printability and mechanical performance while reducing CO_2 emissions.
- The three key factors, including GGBFS content, SP and VMA dosage, were optimised using the TOPSIS-based Taguchi method, resulting in values of 60 % GGBFS content, 5 L/m^3 of SP, and 8 L/m^3 of VMA.
- A flowability value of 180 mm, measured 30 min after adding water to the dry mix, was found to be very appropriate in terms of all other printability performances, such as buildability, deformation, and mini slump value, for the prepared high-volume (60 %) GGBFS mix.
- The study found that OPT mix with an indirect deformation value of 8 %, a mini slump of 3 mm, and a buildability spread diameter of 100 mm exhibited satisfactory buildability performance when conducting direct 3D printing with 20 layers without significant overlapping or buckling. These test results indicate that all the indirect tests to assess printability performance are effective predictors and can be valuable tools for the future research and on-site investigations for preparing and quality assuring of novel 3D printable mixes without requiring a dedicated 3D printing machine.
- The effect of SP and VMA on the printability performance of a 3D printable mix has been found to be very influential. Even a small amount of SP (1 L/m^3) variation can significantly impact overall printability performance. Therefore, it is crucial to apply the optimum dosage of chemical admixtures and maintain it carefully to achieve consistent printability performance.

Based on the successful development of a novel 3D printable mix, the following future research directions are suggested.

- Analysing the mechanical properties of 3D-printed samples, including compressive and flexural strength, with a particular emphasis on anisotropic effects compared to those of mould-cast samples.
- Studying the interlayer bonding by analysing different printing parameters and shrinkage behaviour under various curing conditions using the Optimised 3D printable mix.

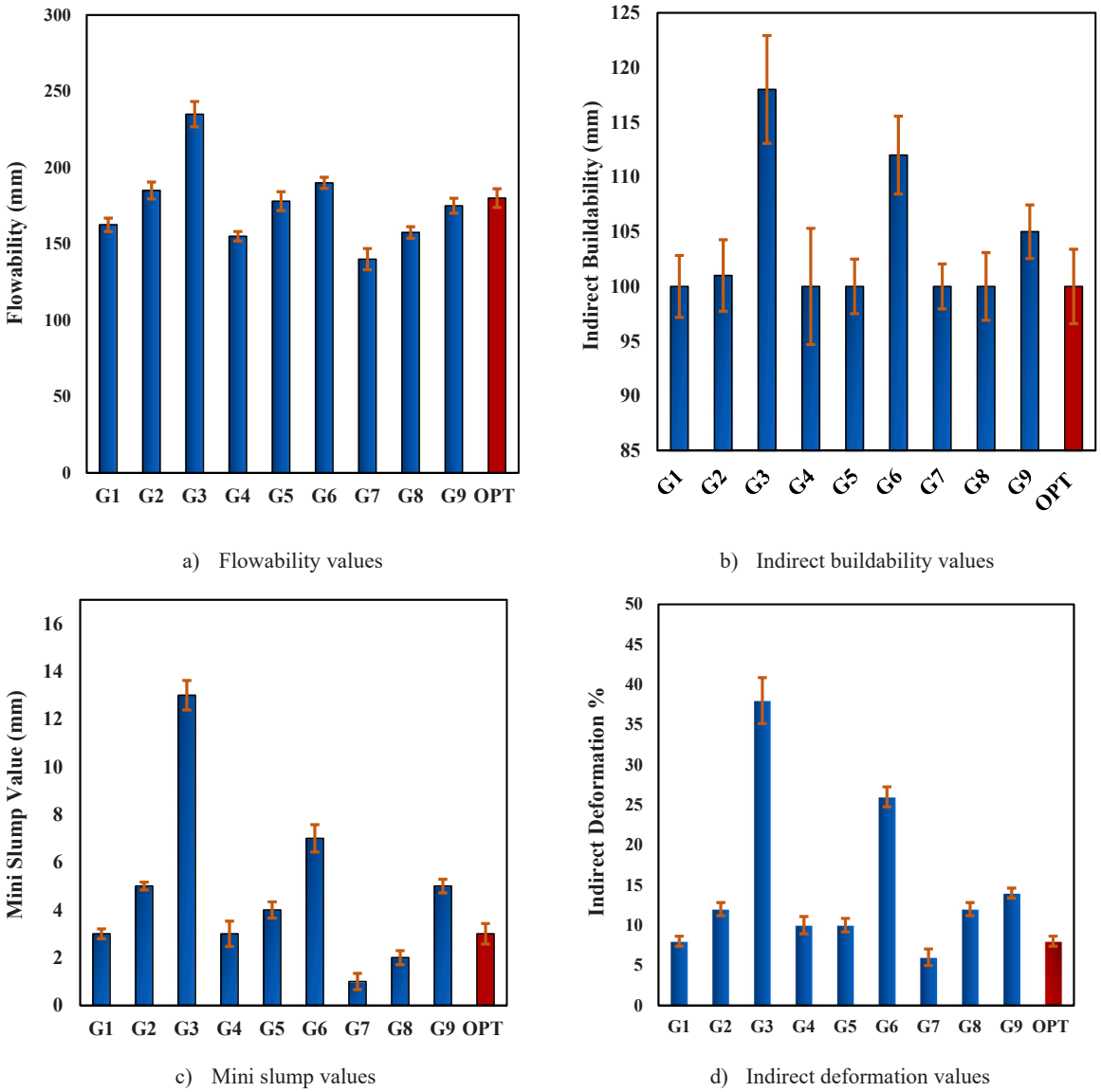

Fig. 8. Fresh property test result.

- Study of various indirect printability tests, as proposed in this study, and establish correlations with direct 3D printed performance. This can help identify optimal ranges for different indirect tests, aiding future researchers who may not have access to 3D printing machines in assessing printability performance.
- Utilizing the proposed TOPSIS based Taguchi method, researchers can explore the performance of different SCMs such as limestone filler, metakaolin, fly ash, and recycled waste powder. Additionally, the effects of different brands of SP and VMA, as well as varying sand-to-binder ratios, can be further investigated.

CRediT authorship contribution statement

Dong An: Investigation, Data curation. **S. Rawat:** Writing – review & editing, Conceptualization. **Mahfuzur Rahman:** Writing – original draft, Investigation, Formal analysis, Data curation, Conceptualization. **Richard (Chunhui) Yang:** Writing – review & editing, Supervision, Methodology, Funding acquisition, Conceptualization. **Y.X. Zhang:** Writing – review & editing, Supervision, Funding acquisition, Conceptualization.

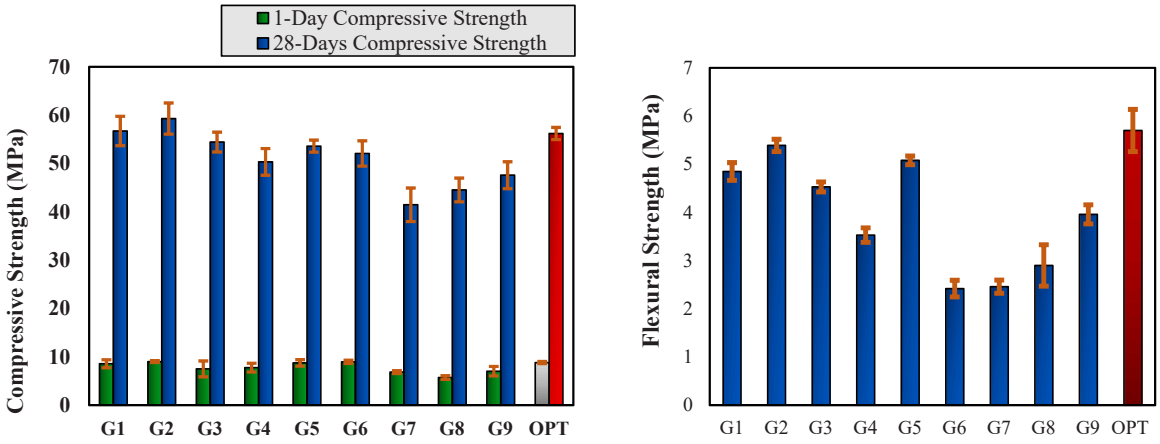

a) Compressive Strength (1-Day & 28-Day) Results b) Flexural Strength (28-Day) Results

Fig. 9. Mechanical property test results.

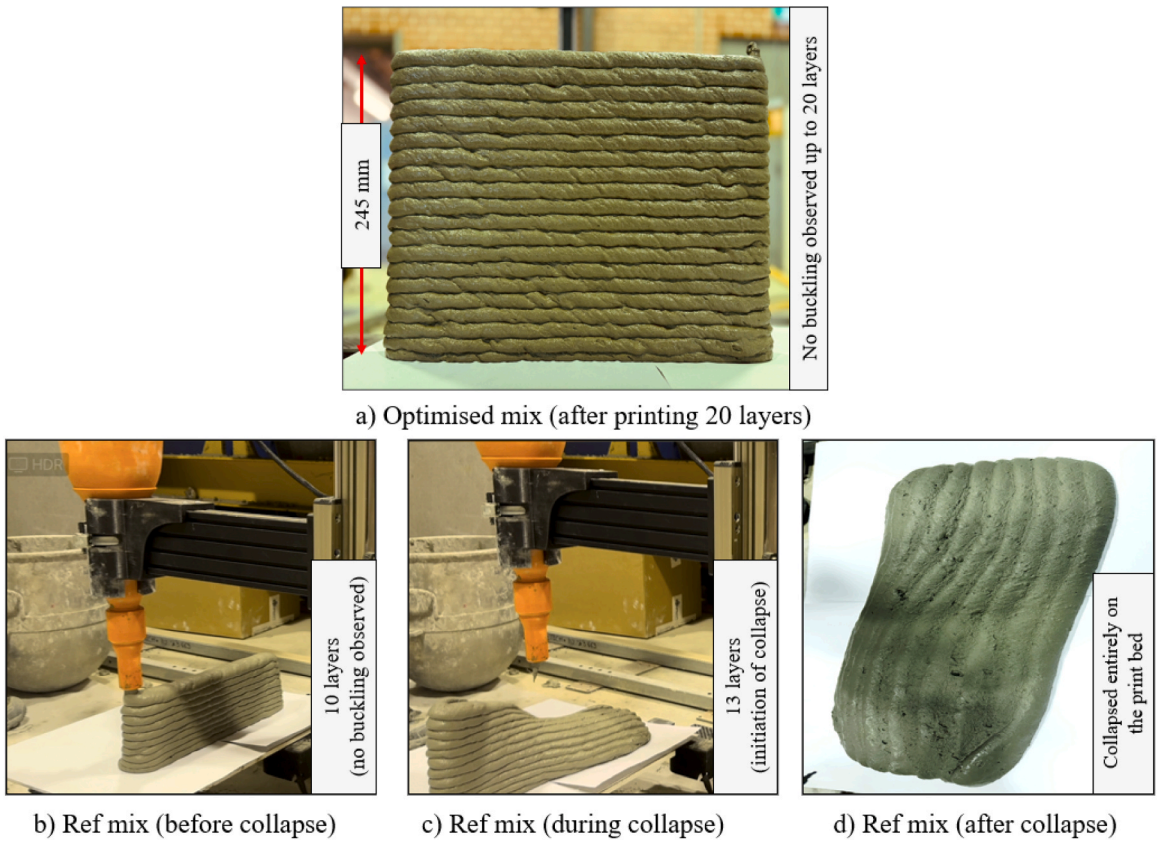

a) Optimised mix (after printing 20 layers)

b) Ref mix (before collapse) c) Ref mix (during collapse) d) Ref mix (after collapse)

Fig. 10. Comparison of 3D printed samples: Optimised mix (a) and reference mix before (b), during (c), and after collapse (d).

Declaration of Competing Interest

The authors declare that they have no known competing financial interests or personal relationships that could have appeared to influence the work reported in this paper.

Acknowledgements

The first and second authors acknowledge financial support on their PhD studies via the Western Sydney University Research Scholarship, funded by Graduate Research School (GRS), Western Sydney University. The second author also acknowledges the PhD scholarship funded by the China Scholarship Council (CSC). The authors are also thankful to the Urban Transformation Research Centre (UTRC), Western Sydney University for providing partial fund for the 3D printer used in this study. Technical support from the Built Environment and Engineering Cluster, the Teaching & Research Technical Services (TRTS), Western Sydney University is appreciated as well.

Data availability

Data will be made available on request.

References

[1] B.A. Ahmed, et al., Printing parameter optimization of additive manufactured PLA using taguchi design of experiment, Polymers 15 (22) (2023) 4370.
[2] G. De Schutter, et al., Vision of 3D printing with concrete—Technical, economic and environmental potentials, Cem. Concr. Res. 112 (2018) 25–36.
[3] G.H. Ahmed, A review of "3D concrete printing": materials and process characterization, economic considerations and environmental sustainability, J. Build. Eng. 66 (2023) 105863.
[4] Y. Chen, et al., A review of printing strategies, sustainable cementitious materials and characterization methods in the context of extrusion-based 3D concrete printing, J. Build. Eng. 45 (2022) 103599.
[5] L. Luo, et al., A multi-objective optimization approach for supply chain design of alum sludge-derived supplementary cementitious material, Case Stud. Constr. Mater. 17 (2022) e01156.
[6] Y. Weng, et al., Design 3D printing cementitious materials via fuller thompson theory and Marson-Percy model, Constr. Build. Mater. 163 (2018) 600–610.
[7] M.A. Moeini, M. Hosseinpoor, A. Yahia, Effectiveness of the rheometric methods to evaluate the build-up of cementitious mortars used for 3D printing, Constr. Build. Mater. 257 (2020) 119551.
[8] B. Panda, et al., The effect of material fresh properties and process parameters on buildability and interlayer adhesion of 3D printed concrete, Materials 12 (13) (2019) 2149.
[9] M.C. Juenger, R. Snellings, S.A. Bernal, Supplementary cementitious materials: new sources, characterization, and performance insights, Cem. Concr. Res. 122 (2019) 257–273.
[10] Y. Liu, et al., Innovative self-healing composites using steel slag and chitosan, Cem. Concr. Compos. 152 (2024) 105652.
[11] H. Ilcan, et al., Rheological properties and compressive strength of construction and demolition waste-based geopolymer mortars for 3D-Printing, Constr. Build. Mater. 328 (2022) 127114.
[12] B. Panda, C. Unluer, M.J. Tan, Investigation of the rheology and strength of geopolymer mixtures for extrusion-based 3D printing, Cem. Concr. Compos. 94 (2018) 307–314.
[13] Z. Xu, et al., Effect of FA and GGBFS on compressive strength, rheology, and printing properties of cement-based 3D printing material, Constr. Build. Mater. 339 (2022) 127685.
[14] M. Rahman, et al., A comprehensive review on fresh and rheological properties of 3D printable cementitious composites, J. Build. Eng. (2024) 109719.
[15] A.U. Rehman, J.-H. Kim, 3D concrete printing: a systematic review of rheology, mix designs, mechanical, microstructural, and durability characteristics, Materials 14 (14) (2021) 3800.
[16] M.S. Barbosa, et al., Development of composites for 3D printing with reduced cement consumption, Constr. Build. Mater. 341 (2022) 127775.
[17] G.B. Omosa, et al., Optimization of open-casting process parameters for fabrication of high-performance TPU/CNT/Fe multi-functional polymer composites: a taguchi with TOPSIS approach, Int. J. Adv. Manuf. Technol. 137 (7) (2025) 3841–3876.
[18] A. Kushwah, et al., Hybrid taguchi-grey relational analysis approach for optimizing cutter operational parameters in selective cauliflower harvesting, Sci. Rep. 14 (1) (2024) 29709.
[19] S. Opricovic, G.-H. Tzeng, Compromise solution by MCDM methods: a comparative analysis of VIKOR and TOPSIS, Eur. J. Oper. Res. 156 (2) (2004) 445–455.
[20] A. C1437, Stand. Test. Method Flow. Hydraul. Cem. Mortar (1999).
[21] A. C230, Standard specification for flow table for use in tests of hydraulic cement, ASTM International, West Conshohocken, PA, 2014.
[22] K. Yu, et al., 3D-printable engineered cementitious composites (3DP-ECC): fresh and hardened properties, Cem. Concr. Res. 143 (2021) 106388.
[23] A. C109, Standard test method for compressive strength of hydraulic cement mortars, ASTM International, 2008.
[24] A. C1609/C1609M, Standard Test Method for Flexural Performance of Fiber-Reinforced Concrete, in, 2012, ASTM International, *West Conshohocken, PA, USA*, 2021, pp. *1–9*.
[25] C.A. Hendriks, et al., Emission reduction of greenhouse gases from the cement industry. Proceedings of the fourth international conference on greenhouse gas control technologies, IEA GHG R&D Programme, Interlaken Austria, 1998.
[26] D.J.M. Flower, J.G. Sanjayan, D. Baweja, Environmental impacts of concrete production and construction. Concrete Institute of Australia-Biennial Conference 2005, Concrete Institute of Australia, 2005.
[27] L. Black, Low clinker cement as a sustainable construction material, Sustain. Constr. Mater. (2016) 415–457.
[28] S. Dumne, Effect of superplasticizer on fresh and hardened properties of self-compacting concrete containing Fly ash, Am. J. Eng. Res. 3 (3) (2014) 205–211.
[29] M. Mathew, S. Sahu, A.K. Upadhyay, Effect of normalization techniques in robot selection using weighted aggregated sum product assessment, Int. J. Innov. Res. Adv. Stud. 4 (2) (2017) 59–63.
[30] S. Rawat, Y. Zhang, C. Lee, Multi-response optimization of hybrid fibre engineered cementitious composite using Grey-Taguchi method and utility concept, Constr. Build. Mater. 319 (2022) 126040.
[31] Q. Yu, et al., Investigation of the rheological and mechanical properties of 3D printed eco-friendly concrete with steel slag, J. Build. Eng. 72 (2023) 106621.
[32] G. Ayim-Mensah, M. Radosavljevic, Influence of ground granulated blast furnace slag on the compressive strength and ductility of ultra High-performance fibre reinforced cementitious composites, Cement 8 (2022) 100030.
[33] R. Jayathilakage, P. Rajeev, J. Sanjayan, Rheometry for concrete 3D printing: a review and an experimental comparison, Buildings 12 (8) (2022) 1190.
[34] A.R. Arunothayan, et al., Rheological characterization of ultra-high performance concrete for 3D printing, Cem. Concr. Compos. 136 (2023) 104854.
[35] E. Booya, et al., The influence of utilizing slag in lieu of Fly ash on the performance of engineered cementitious composites, Constr. Build. Mater. 256 (2020) 119412.